

Trapping Ba^+ with Seven-fold Enhanced Efficiency Utilizing an Autoionizing Resonance

Noah Greenberg, Brendan M. White, Pei Jiang Low, and
Crystal Senko

Institute for Quantum Computing and Department of Physics & Astronomy,
University of Waterloo, Waterloo, Ontario, N2L 3G1, Canada

E-mail: n2greenberg@uwaterloo.ca

Abstract.

Trapped ions have emerged as a front runner in quantum information processing due to their identical nature, all-to-all connectivity, and high fidelity quantum operations. As current trapped ion technologies are scaled, it will be important to improve the efficiency of loading ions, which is currently the slowest process in operating a trapped ion quantum computer. Here, we compare two isotope-selective photoionization schemes for loading $^{138}\text{Ba}^+$ ions. We show that a two-step photoionization scheme ending in an autoionizing transition increases the ion loading rate nearly an order of magnitude compared to an established technique which does not excite an autoionizing state. The only additional technology required to implement the autoionizing transition is a commercial diode laser. Our technique can be extended to all isotopes of barium, and autoionizing resonances exist in every species currently used for trapped ion quantum processing, making this a promising technique to drastically increase the loading rates for all trapped ion computers.

1. Introduction

Barium is a versatile quantum information carrier with the capacity to be used as an optical, metastable, or ground-state qubit [1]. Additionally, barium has been demonstrated as a *qudit*, controlling and reading out up to 13-levels [2] by taking advantage of its unusually long-lived metastable $5d^2D_{5/2}$ state [3]. The flexibility of the atomic structure in barium and the visible wavelengths used to drive the electric-dipole transitions are also attractive from a practical perspective [4]. All of these key features of barium, coupled with extraordinary experimental state-preparation and measurement results [5, 6, 7] has captured the attention of researchers and motivated the trapping of barium in the most sophisticated surface traps as a front-running platform for quantum information processing [8, 9]. Unfortunately, a caveat of working with metallic barium is that it can oxidize within seconds when exposed to atmosphere, and specifically, the $^{133}\text{Ba}^+$ isotope can only be sourced as a salt and used in microgram quantities. For these reasons, the focus of this work is on maximizing the loading rate of barium to

quickly generate long chains of ions for quantum information processing utilizing laser ablation.

Typically, photoionization for trapping ions is done using resonance-enhanced multi-photon ionization [10]. This can involve a resonant “first step”, using a laser that drives an electronic transition in the neutral atom, along with a “second step” using light that is sufficiently energetic to bridge the electron from the excited state to the unbound continuum. Isotope shifts in the first step transition are generally large enough (> 10 MHz) so that only the target isotope of neutral atoms are excited and then ionized. Researchers have employed a variety of different first steps in two-step photoionization schemes for the isotope-selective loading of barium. Some relevant parameters for these first step transitions are outlined in Table 1.

λ (nm)	Intermediate State	Linewidth (MHz)	$6s^2\ ^1S_0$ Branching Ratio
413	$5d\ 6p\ ^3D_1$	9.15 ± 0.26 [11]	0.026(13) [11]
554	$6s\ 6p\ ^1P_1$	19.02 ± 0.19 [11]	0.9966(0.2) [11]
791	$6s\ 6p\ ^3P_1$	0.820 ± 0.050 [12]	0.38 [13]

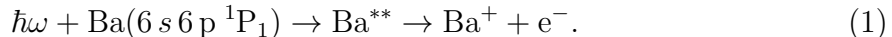
Table 1: Comparison of first steps used to drive a transition in neutral barium between the ground state, $6s^2\ ^1S_0$, and an excited intermediate state, as part of a two-step photoionization process for loading Ba^+ . The branching ratio represents the likelihood that an atom in the intermediate state will decay back to the ground state. In this work we use 554nm as the first step to drive a strong dipole-allowed transition, with a branching ratio almost entirely back down to the ground state.

Utilizing an autoionizing resonance for the second step can significantly enhance the photoionization cross-section [14, 15]. By contrast, previous work loading ions with photoionization has typically used a non-resonant second step (*i.e.* not ending in an autoionizing transition). The non-resonant photoionization scheme ionizes an electron directly into the continuum, while the autoionizing scheme uses a resonant transition to a quasi-bound state embedded in the continuum, providing roughly an order of magnitude higher experimentally measured photoionization cross-section. The probability of trapping is proportional to the photoionization cross-section $P_T \propto \sigma_P$ [16], so by using a more efficient photoionization scheme, the probability of trapping can be increased substantially.

Autoionizing resonances can be found in the ionization spectrum of all elements with two valence electrons, including barium. These resonances, which are found past the first ionization threshold, describe states where the wavefunctions of the electrons have become correlated [17]. They are the result of interference between a discrete state and the ionization continuum [18], and they are found as distinct peaks in the photoionization cross-section. Typically, the resonance is characterized as a Fano-profile [19], allowing useful information to be extracted from the measured cross-section. The

energies and cross sections of these resonances can be calculated with multi-channel quantum defect theory analysis [20, 21, 22] or an eigenchannel R-matrix method [23, 24]. The cross-sections have also been empirically measured [19, 25, 26].

If the photon energy $\hbar\omega$ of the second step is tuned to a known autoionizing resonance, then the two valence electrons will become doubly excited and enter a quasi-bound state Ba^{**} embedded in the ionization continuum with an incredibly short lifetime, $\tau \ll 1$ ns:



In this manuscript, two different photoionization schemes are compared for isotope-selective loading of $^{138}\text{Ba}^+$ ions. Each scheme is a two-step process with the first step using 554 nm light to drive a strong dipole transition between the $6s^2\ ^1S_0 \leftrightarrow 6s6p\ ^1P_1$ states. The second step for ionization uses either a non-resonant photoionization scheme with 405 nm light, or an autoionizing scheme near 390 nm. The two schemes are presented in Fig. 1a. Nearly an order of magnitude increase in loading rate for $^{138}\text{Ba}^+$ ions is observed when using the autoionizing scheme compared with the non-resonant scheme. Furthermore, the autoionizing scheme requires significantly lower amounts of optical power in the second step to trap long chains of $^{138}\text{Ba}^+$, which reduces the likelihood of trap charging. The observed increase in loading rates is consistent with the increase in the previously experimentally measured photoionization cross-sections of the two compared photoionization schemes [19, 25, 26].

2. Experimental Overview

The comparison of the two different photoionization schemes was conducted on a four-rod trap using IonControl software [27]. These experiments are performed using laser ablation on a natural abundance, stable, salt (BaCl_2) target in an isotope-selective manner with a two-step photoionization process to trap $^{138}\text{Ba}^+$ [28]. As depicted in Fig. 1b, the trap is comprised of four electropolished tungsten rods with 0.5 mm diameter and two chemically-etched needles separated by 2.8 mm, which act as the end caps. Typically, $V_{DC} = 7 - 9$ V are applied to the needles, providing axial confinement of the ions. The voltage applied to the rods is $|V_{RF}| \approx 230$ V delivered at $\nu_{RF} = 20.772$ MHz by a helical resonator [29].

There are three relevant beam paths as depicted in Figure 1b. The first beam path is comprised of linearly polarized 493, 554, and 650 nm light focused to beam radii of $\approx 31, 35, 41$ μm , respectively. This path provides Doppler cooling via 493 nm using the $6s\ ^2S_{1/2} \leftrightarrow 6p\ ^2P_{1/2}$ transition, with 650 nm light used to repump $5d\ ^2D_{3/2} \rightarrow 6p\ ^2P_{1/2}$. The 554 nm laser is used to drive the first step in the photoionization process. The usual laser powers are $110 \pm 3, 15 \pm 1, \text{ and } 210 \pm 6$ μW for the 493, 554, and 650 nm beams, respectively.

The second beam path consists of linearly polarized 390 or 405 nm light, as well as 614 nm light. This path intersects with the first beam path at the center of the trap,

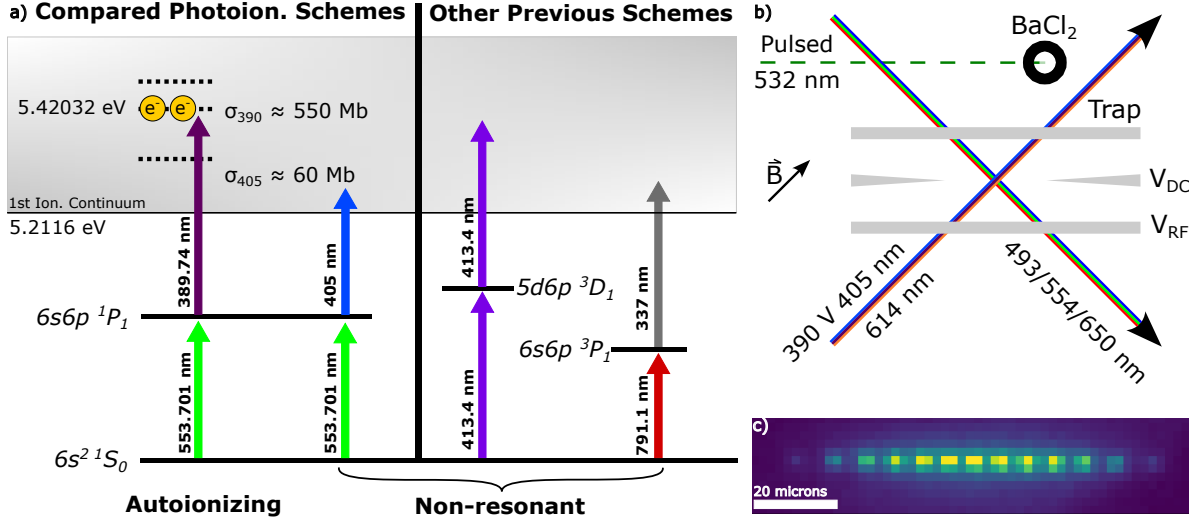


Figure 1: a) Comparison of the two different photoionization schemes in the text, with the previously measured cross-sections σ_{390} and σ_{405} [19]. Each scheme uses the exact same first step, exciting neutral barium to the $6s6p\ ^1P_1$ state. The second step varies depending on the scheme, either ending in an autoionizing resonance or somewhere in the continuum not resonant with a specific transition. Autoionizing states are represented by dashed lines in the continuum. b) Experimental overview of the beam geometry. The 554 nm beam is orthogonal to the atomic plume to reduce Doppler broadening and also orthogonal to the second ionization beam (either 390 or 405 nm) to reduce the ionization volume. c) A chain of thirteen $^{138}\text{Ba}^+$ ions trapped with a single ablation pulse using the autoionizing scheme. The outer ions sit far from the center of the beam, causing them to be dim compared to the center ions. Each pixel is $\approx 2\ \mu\text{m}$.

$\approx 0.707\ \text{mm}$ from the trap rods. During any given experiment either 390 nm or 405 nm was used as the second photoionization step, but never both. In Ba^+ , the $5d\ ^2D_{5/2}$ state is populated within a few seconds of exposure to the 390 nm laser, because the 390 nm beam is detuned by $< 1\ \text{nm}$ from the $6p\ ^2P_{1/2} \rightarrow 6d\ ^2D_{3/2}$ transition. This can decay to $5d\ ^2D_{5/2}$, so the 614 nm laser is used to repump $5d\ ^2D_{5/2} \rightarrow 6p\ ^2P_{3/2}$. The 614 nm beam carries $7 \pm 1\ \mu\text{W}$ of power. It should be noted that the 614 nm is not necessary if the 390 nm beam is shuttered shortly after trapping. In this set of experiments, the 390 nm was not shuttered so the 614 nm was required for efficient cooling and ion detection. The beam radii were $\approx 34\ \mu\text{m}$ and $\approx 35\ \mu\text{m}$ for the 390 nm and 405 nm beams, respectively. The powers of the 390 nm and 405 nm beams vary depending on the experiment, but we only observe trapping above $150\ \mu\text{W}$ in this setup using either laser.

As shown in Fig. 1b, the third and final beam consists of only the 532 nm ablation laser. This is a nanosecond pulsed, flash-lamp pumped, Nd:YAG laser, capable of delivering up to 10 mJ of pulse energy, although we operate in practice at much lower pulse energies, around 140 μJ . Upon hitting the ablation target, this laser pulse causes sublimation of the BaCl_2 , generating a vapor of atomic barium. The ablation target is oriented such that the surface norm is directed towards the trap center, 14.6 mm away

[28], with the atomic plume reaching the trap within 10 – 15 μs . The target contains 40 – 50 mg worth of BaCl_2 .

The 405 nm laser is a fiber-pigtailed Cobolt 06-MLD from HÜBNER Photonics GmbH. The 390 nm laser is a tunable Littrow laser from MOGLabs. In practice, neither of these lasers were frequency locked, although the 390 nm has the ability to be locked using a wavemeter. The frequencies of the first step for each isotope have already been measured in previous works [28]. For trapping $^{138}\text{Ba}^+$, the 554 nm laser is locked to 553.701 85 nm. The optimal wavelength of the second step is calculated to be 389.747 79 nm based on the first step and the previously measured photoionization cross-sections [30], where the autoionizing resonance occurs 5.420 32 eV above the $6\text{s}^2\text{S}_0$ state. The resonance is > 50 GHz wide, which exceeds the mode-hop free tuning range of the 390 nm Littrow laser, so no attempt was made to rigorously quantify the loading rate as a function of frequency. In these experiments, the 390 nm laser was simply tuned to 389.748 ± 0.01 nm, and a significant increase in the loading rate of $^{138}\text{Ba}^+$ was observed, which is detailed in the following sections.

For ablation loading of the ion trap, the following experimental procedure is employed:

- (i) The RF and DC trap voltages are turned on and the laser frequencies are set for $^{138}\text{Ba}^+$.
- (ii) The ablation laser sends a single pulse to the target. Approximately, 10 – 15 μs later, the majority of the atomic flux reaches the trapping region where the atoms either pass through or are photoionized by the two-step process.
- (iii) Doppler cooling sweeps are implemented in order to cool and crystallize hot ions that may have been trapped. This is done by red-detuning the 493 nm cooling beam 100 – 500 MHz and sweeping within five seconds back to the nominal cooling frequency.
- (iv) Steps (i)-(iii) are repeated until an ion is trapped.

Fluorescent light from neutral atoms and ions is collected by a 0.26 NA home-built objective and sent to either a photo-multiplier tube (H10682-210) or a charge-coupled device (BFLY-PGE-05S2M-CS). Typically, experiments were run with light being sent to the photo-multiplier tube to quickly determine whether an ion had been trapped. To count how many ions were trapped, the collected light is sent to the charge-coupled device to image the ion chain, as shown in Fig. 1c.

3. Results

3.1. Saturation Intensity & Fluence Experiments

The following section compares the loading rates utilizing the two photoionization schemes as the second step power is varied. We find that the loading rates saturate in the autoionizing scheme at much lower powers compared to the non-resonant scheme.

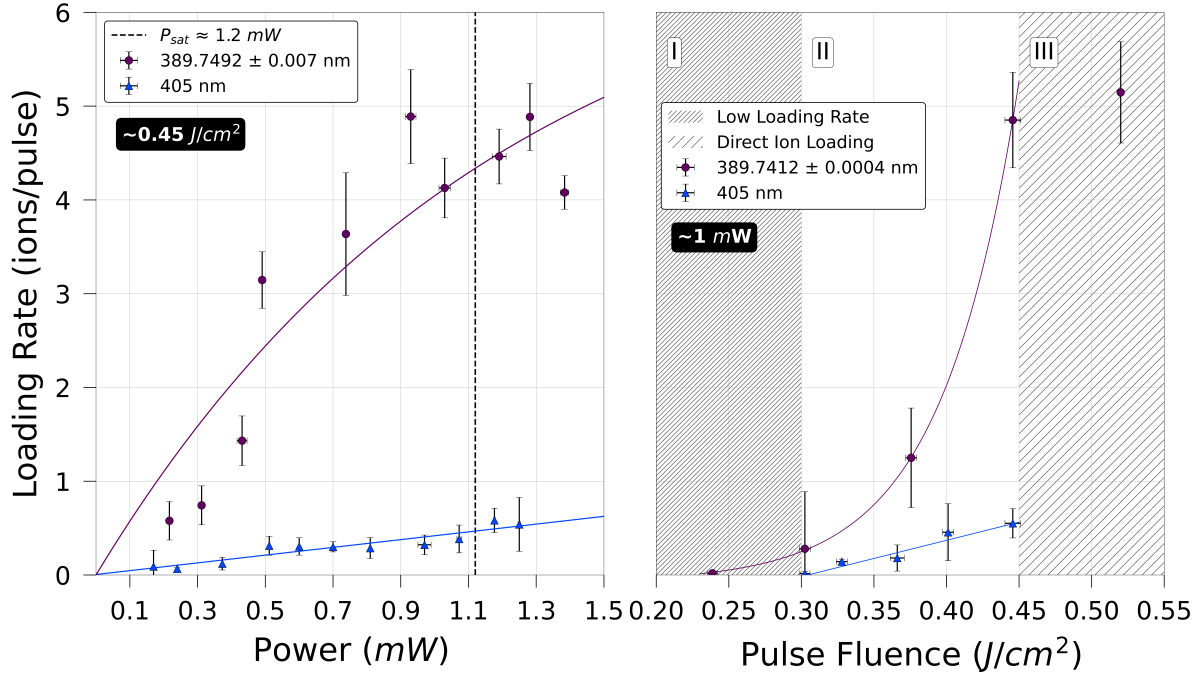


Figure 2: a) Loading rates of $^{138}\text{Ba}^+$ as a function of power carried by the second step laser in the two-step photoionization process. The calculated P_{sat} of the autoionizing transition is denoted by the dashed line. The fit to the autoionizing transition assumes the loading rate follows an exponential of the type $f(x) = a(1 - e^{-b \cdot x})$, where $a = 7.10 \pm 0.06$ ions/pulse and $b = 0.84 \pm 0.04 \text{ mW}^{-1}$ are fitted constants and x is power in milliwatts [25]. The fit predicts $f(1/b) \approx 4.5$, which agrees well with the calculated saturation parameter $f(P_{sat}) \approx 4.4$. The fit to the non-resonant 405 nm loading rate is linear. The error bars represent the standard error of the mean. The ablation fluence was $\approx 0.45 \text{ J cm}^{-2}$. b) Loading rates of $^{138}\text{Ba}^+$ as a function of ablation fluence. We operate primarily in Region II. The regions are described further in the text. The power carried by the second step photoionization beam was $\approx 1 \text{ mW}$. The fitted lines act simply as visual guides.

Similarly, we vary the ablation fluence and find that the autoionizing scheme can load ions with significantly lower neutral flux. Typically, we work with laser powers on the second-step photoionization beam of up to a milliwatt. In this regime, the photoionization cross-section in non-resonant schemes is so small that the loading rate scales linearly. In comparison, autoionizing schemes have quite a large photoionization cross-section with similar amounts of power and the ionization efficiency can reach near 100% [31].

The loading rates of $^{138}\text{Ba}^+$ (ions/pulse) as a function of laser powers for both photoionization schemes are depicted in Fig. 2a. Below $200 \mu\text{W}$ the autoionizing and non-resonant photoionization schemes converge to a loading rate of zero. But at higher powers, the autoionizing transition saturates and the loading rate utilizing the autoionizing transition significantly outperforms that of the non-resonant scheme.

Saturation of the autoionizing transition occurs at relatively low laser power ≈ 1.2 mW with a loading rate of roughly 5 ions/pulse. Based on a linear fit, the non-resonant scheme is predicted to require at least ≈ 12 mW of power to achieve a similar loading rate with a similar beam size as the 390 nm.

The saturation power P_{sat} for the autoionizing transition is calculated using the fitted Fano linewidth parameter $\Gamma \approx 60.4 \pm 1$ GHz [19] and saturation intensity $I_{sat} = \frac{\hbar\omega^3\Gamma}{4\pi c^2} \approx 63.7$ W cm $^{-2}$, where c is the speed of light and $\omega = 2\pi \cdot 769.211$ THz is the angular frequency of the light. With our beam radius of $w_0 = 34$ μ m for the 390 nm beam, the saturation power P_{sat} is calculated to be:

$$P_{sat} = \frac{I_{sat}w_0^2\pi}{2} \approx 1.2 \text{ mW}. \quad (2)$$

We were able to achieve saturation on this transition, as shown in Figure 2a, and our results agree well with the calculated saturation. The ablation laser pulse fluence was kept constant throughout the saturation experiments at 0.45 ± 0.01 J cm $^{-2}$.

Fig. 2b. shows the loading rate of $^{138}\text{Ba}^+$ as a function of ablation laser fluence. The ablation laser fluence experiments were conducted with 1.02 ± 0.02 and 1.20 ± 0.04 mW of average power on the 405 nm and 390 nm beams, respectively. As the laser fluence increases so does the amount of neutral atoms and ions produced. If the fluence is too low, loading can be difficult, but if it is too high, ions can be trapped directly [28]. There are three main regions considered when conducting the ablation loading experiments. Region I (< 0.3 J cm $^{-2}$) is a region of low laser fluence in which there is minimal loading of $^{138}\text{Ba}^+$ ions. We were not able to load in this region using the non-resonant scheme after 100 attempts; however, we were able to successfully load after 53 attempts using the autoionizing scheme. Region II ($0.3 - 0.45$ J cm $^{-2}$) is the ideal operating fluence for trapping, since it produces enough neutral atom flux to trap in an isotope-selective manner, but not enough ablation-produced ions to load directly. Region III (> 0.45 J cm $^{-2}$) is a region of high fluence which produces a significant amount of ions from the ablation process itself, drastically reducing isotope-selectivity since ions can be loaded directly into the trap. These regions are not hard limits, but act mostly as guidelines for these experiments conducted with a BaCl $_2$ ablation target.

3.2. Optimized Loading Rates

In this section, we compare the loading rates of $^{138}\text{Ba}^+$ with ideal laser parameters. For these experiments, the ablation fluence was set to 0.45 J cm $^{-2}$ and the average powers of the second step 405 and 390 nm photoionizing beams were $P_{390} = 1.08 \pm 0.01$ and $P_{405} = 1.17 \pm 0.01$ mW, respectively.

The likelihood of trapping long chains of $^{138}\text{Ba}^+$ was greatly increased using the autoionizing scheme, which is evident by the increase in the average ions per pulse. Roughly one out of five attempts succeeded in trapping using the non-resonant scheme, while nine out of ten attempts succeeded using the autoionizing scheme. The average

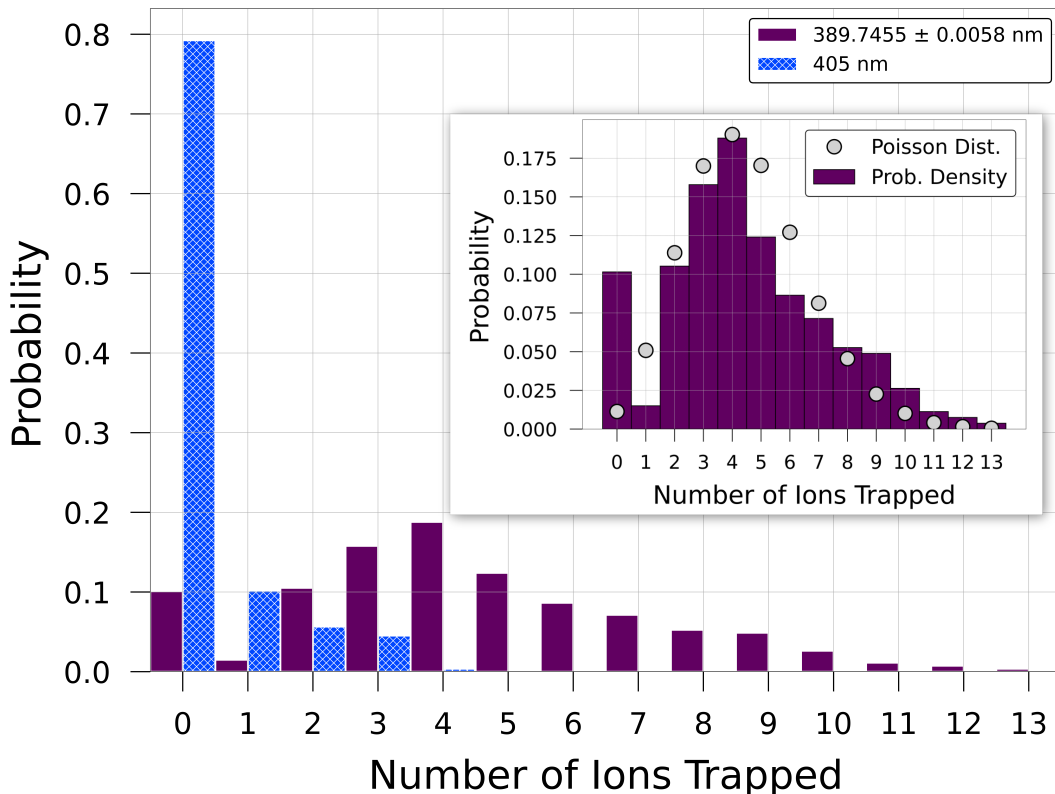


Figure 3: Histogram of the loading rates of $^{138}\text{Ba}^+$, where each event is a single ablation pulse and trapping attempt. The average loading rate using the autoionizing scheme was $R_{390} = 4.48 \pm 0.17$ ions/pulse and the average loading rate using the non-resonant scheme was $R_{405} = 0.43 \pm 0.11$ ions/pulse. There were 265 and 266 trapping attempts for the non-resonant and autoionizing scheme, respectively. The inset shows the probability of loading using the autoionizing scheme fitted to a Poisson distribution.

loading rates with the standard error of the mean are $R_{405} = 0.43 \pm 0.11$ ions/pulse and $R_{390} = 4.48 \pm 0.17$ ions/pulse using the non-resonant and autoionizing schemes, respectively. These rates are compared in Fig. 3. The median ions trapped per pulse was 0 ions for the non-resonant scheme and 4 ions for the autoionizing scheme.

The loading rates quoted above cannot be directly compared to infer the enhancement from the autoionizing resonance, because the powers of the second-step lasers and the quantity of neutral atoms produced during ablation were not identical across both sets of experiments. During the loading experiments, we monitor the rate of fluorescence at 554 nm after each ablation laser pulse, as a proxy for the flux of neutral barium atoms. We observed higher neutral atom flux for the experiments conducted with the autoionizing scheme than with the non-resonant scheme (up to 39.5% higher fluorescence counts at 554 nm), which we attribute to natural variations in the number of ablated atoms. We make the simplifying assumptions that the probability of trapping is proportional to both the neutral atom flux and the average second-step laser power, when the ionization rate is far from saturation [28]. Thus, we estimate

that the loading rate using 405 nm would have been $R'_{405} = 0.66 \pm 0.24$ ions/pulse, if the neutral atom flux and second-step laser power had been identical to those in the 390 nm experiments. We therefore calculate that the increase in loading rate of $^{138}\text{Ba}^+$ using the autoionizing scheme is a factor of $R_{390}/R'_{405} \approx 6.8 \pm 2.7$. This compares well with the ratio of photoionization cross-sections, which have previously been measured as $\sigma_{390}/\sigma_{405} = 520 \text{ Mb}/75 \text{ Mb} \approx 6.9$ [19] and $550 \text{ Mb}/60 \text{ Mb} \approx 9.2$ [26].

4. Discussion

The demonstrated autoionizing scheme using 554 and 390 nm retains the isotope-selectivity previously presented in [28], since it utilizes the same first step, which is the isotope-selective step in the photoionization process. We conducted a brief study to confirm this, where 478 ions (minimum of two $^{138}\text{Ba}^+$ ions in the chain, a total of 114 unique ion chains) were analyzed for dark or dim ions, which indicate the presence of other ion isotopes besides $^{138}\text{Ba}^+$. We found that only 8 ions in all of these chains were other isotopes. This puts a maximum bound on the isotope-selectivity for $^{138}\text{Ba}^+$ of 98%, which is consistent with previous studies [28]. To achieve high loading rates, the first transition in the ionization sequence is usually power broadened significantly, which limits isotope selectivity [28]. Thus, using this more efficient autoionizing scheme and lowering the power of the first step laser may allow for better isotope selectivity with similar loading rates in the future.

We briefly investigated the loading rates of the $^{137}\text{Ba}^+$ isotope with the autoionizing scheme. A significant increase in the loading rate, with a factor of at least 5, was immediately apparent for the autoionizing scheme. However, we did not make a controlled quantitative comparison between the two schemes for this isotope. This photoionization scheme can also be applied to $^{133}\text{Ba}^+$ since the autoionizing transition is broad enough that it makes any isotope shifts between $^{138}\text{Ba}^+$, $^{137}\text{Ba}^+$, and $^{133}\text{Ba}^+$ negligible.

The linewidth of the measured autoionizing resonance is ≈ 60 GHz, but we found a considerable increase in the loading rate even when the frequency of the 390 nm laser was > 100 GHz detuned from the 389.747 79 nm transition. So in practice, tuning anywhere near this resonance can result in a significant increase in the loading rate. In fact, the autoionizing transition is so broad that precision control of the laser frequency and linewidth are not required.

There are many autoionizing resonances embedded in the first ionization continuum of barium that can be used for efficient photoionization. Assuming 554 nm is the first step in a two-step photoionization scheme, the best second step is to utilize the strongest autoionizing resonance, as this will most efficiently ionize the neutral atoms and allow for smaller amounts of optical power to be used. Other possible autoionizing states that are easily accessible from the intermediate $6s6p\ ^1P_1$ state are outlined in Table 2.

Other first steps can be used besides 554 nm to drive to an intermediate state before exciting an autoionizing state embedded in the continuum. This includes, but

Wavelength (nm)	Cross-section (Mb)	Autoion. State [30]	Energy (eV) [19]
380.75	≈ 300 [19]	$5 d_{3/2} 9 d (J = 0)$	5.49549
384.33	≈ 290 [19]	$5 d_{3/2} 9 d (J = 1)$	5.46516
389.74	550 [19], 520 ± 78 [26]	$5 d_{5/2} 8 d (J = 1)$	5.42032
402.92	370 [19], 300 ± 45 [26]	$5 d_{3/2} 8 d (J = 1)$	5.31629

Table 2: Comparison of some previously measured autoionizing resonances when using $6s6p\ ^1P_1$ as the intermediate state. Other intermediate states can be used, but the highest experimentally measured photoionization cross-section of barium utilizes $6s6p\ ^1P_1$ as the intermediate state. The energy is relative to the $6s^2\ ^1S_0$ ground state.

is not limited to, the $5d6p\ ^3D_1$ state driven with 413 nm light [32] and the $6s6p\ ^3P_1$ state driven with 791 nm light [26]. The highest resonance in the photoionization cross-section utilizing the $6s6p\ ^3P_1$ intermediate state has been measured to be 102 ± 15 Mb using 340 nm as the second step [26]. This is a significantly strong resonance, but still considerably lower than the 550 Mb cross-section using $6s6p\ ^1P_1$ as the intermediate state with 390 nm. There are considerable resonances in the photoionization spectrum of barium using $5d6p\ ^3D_1$ as an intermediate state, for which relative cross-sections have been measured [32].

5. Conclusion

We have demonstrated an efficient isotope-selective photoionization scheme for trapping barium ions utilizing an autoionizing resonance, motivated by the elusive $^{133}\text{Ba}^+$ and $^{137}\text{Ba}^+$ isotopes. The increase in loading rates (ions/pulse) compared with previous ablation studies are consistent with previously measured photoionization cross-sections of barium and equate to nearly an order of magnitude increase in the loading rate of $^{138}\text{Ba}^+$ ions. This photoionization scheme will aid in the consistent trapping of long chains of barium ions and will help enable NISQ era devices to be built based on rare isotopes like $^{133}\text{Ba}^+$. Furthermore, the demonstrated advantage of utilizing autoionizing resonances allows researchers to efficiently ionize neutral atoms without having to focus significant amounts of power near the trap, reducing the risk of trap charging.

Acknowledgments

This research was supported in part by the Natural Sciences and Engineering Research Council of Canada (NSERC) and the Canada First Research Excellence Fund (CFREF). We would like to thank Dr. Jens Lassen, a research scientist at TRIUMF, for his initial suggestion and for pointing out the existence of these autoionizing resonances as well as ongoing discussion related to the experiment. We thank Dr. Akbar Jahangiri Jozani, Nicholas Zutt, and Xinghe Tan for reviewing the manuscript.

Conflict of interest

The authors declare no conflicts of interest.

- [1] D. T. C. Allcock, W. C. Campbell, J. Chiaverini, I. L. Chuang, E. R. Hudson, I. D. Moore, A. Ransford, C. Roman, J. M. Sage, and D. J. Wineland. omg blueprint for trapped ion quantum computing with metastable states. *Applied Physics Letters*, 119(21), 11 2021. 214002.
- [2] Pei Jiang Low, Brendan White, and Crystal Senko. Control and readout of a 13-level trapped ion qudit, 2023.
- [3] A. A. Madej and J. D. Sankey. Quantum jumps and the single trapped barium ion: Determination of collisional quenching rates for the $5d^2D_{5/2}$ level. *Phys. Rev. A*, 41:2621–2630, 3 1990.
- [4] Ali Binai-Motlagh, Matthew Day, Nikolay Videnov, Noah Greenberg, Crystal Senko, and Rajibul Islam. A guided light system for agile individual addressing of ba^+ qubits with 10^{-4} level intensity crosstalk, 2023.
- [5] D. Hucul, J. E. Christensen, Eric R. Hudson, and Wesley C. Campbell. Spectroscopy of a synthetic trapped ion qubit. *Phys. Rev. Lett.*, 119:100501, 9 2017.
- [6] J. E. Christensen. *High-fidelity operation of a radioactive trapped ion qubit*, ^{133}Ba . PhD thesis, University of California, Los Angeles, 2020.
- [7] Fangzhao Alex An, Anthony Ransford, Andrew Schaffer, Lucas R. Sletten, John Gaebler, James Hostetter, and Grahame Vittorini. High fidelity state preparation and measurement of ion hyperfine qubits with $i > \frac{1}{2}$. *Phys. Rev. Lett.*, 129:130501, 9 2022.
- [8] X. Shi, S. L. Todaro, G. L. Mintzer, C. D. Bruzewicz, J. Chiaverini, and I. L. Chuang. Ablation loading of barium ions into a surface electrode trap, 2023.
- [9] R. D. Graham, S.-P. Chen, T. Sakrejda, J. Wright, Z. Zhou, and B. B. Blinov. A system for trapping barium ions in a microfabricated surface trap. *AIP Advances*, 4(5):057124, 2014.
- [10] Michael N.R. Ashfold and Colin M. Western. Multiphoton spectroscopy, applications. In John C. Lindon, editor, *Encyclopedia of Spectroscopy and Spectrometry*, pages 1424–1433. Elsevier, Oxford, 1999.
- [11] S. Niggli and M. C. Huber. Transition probabilities in neutral barium. *Phys. Rev. A*, 35(7):2908–2918, 1987.
- [12] A.M. Akulshin, A.A. Celikov, and V.L. Velichansky. Nonlinear doppler-free spectroscopy of the $61s0-63p1$ intercombination transition in barium. *Optics Communications*, 93(1):54–58, 1992.
- [13] V. A. Dzuba, V. V. Flambaum, and J. S. M. Ginges. Calculation of parity and time invariance violation in the radium atom. *Phys. Rev. A*, 61:062509, May 2000.
- [14] A. G. Shenstone. Ultra-ionization potentials in mercury vapor. *Phys. Rev.*, 38:873–875, 9 1931.
- [15] K. Vant, J. Chiaverini, W. Lybarger, and D. J. Berkeland. Photoionization of strontium for trapped-ion quantum information processing, 2006.
- [16] L. Deslauriers, M. Acton, B. B. Blinov, K.-A. Brickman, P. C. Haljan, W. K. Hensinger, D. Hucul, S. Katnik, R. N. Kohn, P. J. Lee, M. J. Madsen, P. Maunz, S. Olmschenk, D. L. Moehring, D. Stick, J. Sterk, M. Yeo, K. C. Younge, and C. Monroe. Efficient photoionization loading of trapped ions with ultrafast pulses. *Phys. Rev. A*, 74:063421, 12 2006.
- [17] U Fano. Correlations of two excited electrons. *Reports on Progress in Physics*, 46(2):97, 2 1983.
- [18] U. Fano. Effects of configuration interaction on intensities and phase shifts. *Phys. Rev.*, 124:1866–1878, 12 1961.
- [19] B Willke and M Kock. Measurement of photoionization cross sections from the laser-excited $\text{ba i (6s6p) 1p}_{10}$ state. *Journal of Physics B: Atomic, Molecular and Optical Physics*, 26(6):1129, 3 1993.
- [20] M Aymar. Eigenchannel r-matrix calculation of the $j=1$ odd-parity spectrum of barium. *Journal of Physics B: Atomic, Molecular and Optical Physics*, 23(16):2697, 8 1990.
- [21] M Aymar and O Robaux. Multichannel quantum-defect analysis of the bound even-parity $j=2$ spectrum of neutral barium. *Journal of Physics B: Atomic and Molecular Physics*, 12(4):531,

2 1979.

- [22] Mireille Aymar, Chris H. Greene, and Eliane Luc-Koenig. Multichannel rydberg spectroscopy of complex atoms. *Rev. Mod. Phys.*, 68:1015–1123, 10 1996.
- [23] Chris H. Greene and Constantine E. Theodosiou. Photoionization of the ba 6s6p 1p_1 state. *Phys. Rev. A*, 42:5773–5775, 11 1990.
- [24] Chris H. Greene and Mireille Aymar. Spin-orbit effects in the heavy alkaline-earth atoms. *Phys. Rev. A*, 44:1773–1790, 8 1991.
- [25] L.-W. He, C. E. Burkhardt, M. Ciocca, J. J. Leventhal, and S. T. Manson. Absolute cross sections for the photoionization of the 6s6p 1p excited state of barium. *Phys. Rev. Lett.*, 67:2131–2134, 10 1991.
- [26] M. M. Ali Kalyar. *Two-step Laser Excitation Studies of Bound and Autoionizing States in Barium*. PhD thesis, Quaid-i-Azam University, Islamabad, 2008.
- [27] Peter Maunz, Jonathan Mizrahi, and Josh Goldberg. Ioncontrol v. 1.0, version 00, 6 2016.
- [28] Brendan M. White, Pei Jiang Low, Yvette de Sereville, Matthew L. Day, Noah Greenberg, Richard Rademacher, and Crystal Senko. Isotope-selective laser ablation ion-trap loading of $^{137}\text{Ba}^+$ using a bacl_2 target. *Phys. Rev. A*, 105:033102, 3 2022.
- [29] P. J. Low. Tolerable experimental imperfections for a quadrupole blade ion trap and practical qudit gates with trapped ions. Master’s thesis, University of Waterloo, 2019.
- [30] P Camus, M Dieulin, A El Himdy, and M Aymar. Two-step optogalvanic spectroscopy of neutral barium: Observation and interpretation of the even levels above the 6s ionization limit between 5.2 and 7 eV. *Physica Scripta*, 27(2):125, 2 1983.
- [31] M. G. Payne and G. S. Hurst. *Theory of Resonance Ionization Spectroscopy*, pages 183–188. Springer US, Boston, MA, 1985.
- [32] Darrell J. Armstrong, Robert P. Wood, and Chris H. Greene. Photoionization of the 5d6p 3d_1 state of barium. *Phys. Rev. A*, 47:1981–1988, Mar 1993.